Rafaela de Paula Silva

Correction Strategy for Wear-out Prediction of Photovoltaic Inverters Considering the Mission Profile Resolution Effects

Viçosa, MG

2020

Rafaela de Paula Silva

Correction Strategy for Wear-out Prediction of Photovoltaic Inverters Considering the Mission Profile Resolution Effects

Monografia apresentada ao Departamento de Engenharia Elétrica do Centro de Ciências Exatas e Tecnológicas da Universidade Federal de Viçosa, para a obtenção dos créditos referentes à disciplina ELT 402 - Projeto de Engenharia II e cumprimento do requisito parcial para obtenção do grau de Bacharel em Engenharia Elétrica.

Universidade Federal de Viçosa

Departamento de Engenharia Elétrica

Curso de Graduação em Engenharia Elétrica

Orientador: Prof. Dr. Heverton Augusto Pereira

Coorientador: Me. Rodrigo Cassio de Barros

Viçosa, MG

2020

Rafaela de Paula Silva

Correction Strategy for Wear-out Prediction of Photovoltaic Inverters Considering the Mission Profile Resolution Effects

Monografia apresentada ao Departamento de Engenharia Elétrica do Centro de Ciências Exatas e Tecnológicas da Universidade Federal de Viçosa, para a obtenção dos créditos referentes à disciplina ELT 402 - Projeto de Engenharia II e cumprimento do requisito parcial para obtenção do grau de Bacharel em Engenharia Elétrica.

Trabalho aprovado. Viçosa, MG, 18 de dezembro de 2020:

Prof. Dr. Heverton Augusto Pereira
Orientador

Me. Rodrigo Cassio de Barros
Coorientador

Me. Renata Oliveira de Sousa
Convidado 1

Eng. Eletricista João Marcus Soares Callegari
Convidado 2

Viçosa, MG
2020

A Deus, minha família, mentores e amigos.

Agradecimentos

Em primeiro lugar, obrigada Deus por sempre e incondicionalmente se fazer presente em minha vida, me concedendo a força e disposição necessárias para enfrentar os desafios do dia a dia. Grata a Ti sou todos os dias, mas aqui agradeço, especialmente, por ter me iluminado durante a confecção deste trabalho, permitindo que o mesmo pudesse ser finalizado.

Agradeço imensamente aos meus pais, Sandra e José Caetano, por todo o amor recebido durante todos os dias de minha vida. Vocês são fonte de confiança, determinação, carinho, zelo e perseverança para mim. Obrigada pelo incondicional apoio e por sempre se fazerem presentes em meus dias. A execução deste trabalho certamente não teria sido possível sem a compreensão e suporte que recebo de vocês. Todas as minhas conquistas são frutos do exemplo que encontro em vocês.

Agradeço também à minha irmã, Priscila, que sempre foi uma das maiores inspirações de minha vida. Obrigada por me mostrar e me fazer acreditar que tenho potencial para chegar onde quero. Um dia você transformou uma de minhas maiores dificuldades em uma de minhas maiores motivações ao dizer que eu deveria me sentir mais forte que os outros por ser tão tímida. Isso porque, segundo você, enquanto todos os outros vencem uma batalha por dia, eu venço duas, porque começo vencendo a minha própria timidez. Eu não te contei, mas essa frase mudou minha vida. Estou com muitas saudades de você Pri.

Agradeço à Universidade Federal de Viçosa e ao corpo docente do Departamento de Engenharia Elétrica por todo o processo de minha formação acadêmica. Agradeço, em especial, ao grupo de pesquisa GESEP, onde tive oportunidades imensuráveis de crescimento profissional e acadêmico. Agradeço ao meu orientador prof. Heverton por toda sua competência e conhecimentos compartilhados. Suas ideias foram de fundamental importância para a construção deste trabalho. Agradeço também ao prof. Allan que tanto contribuiu para a minha evolução acadêmica.

Ao meu coorientador Rodrigo, com quem tive o imenso prazer de trabalhar diretamente e rotineiramente, deixo um agradecimento especial. Obrigada por toda a parceria e por compartilhar tanto comigo. Você com certeza é um dos maiores contribuintes da evolução profissional e pessoal que venho vivenciando nos últimos anos. Esse projeto é fruto do nosso trabalho árduo que combinou perseverança, sintonia, paciência, persistência e também amizade. Só tenho a agradecer por tudo que aprendi e cresci trabalhando com você. Me inspiro na pessoa e profissional incríveis que você é.

Por último, mas não menos importante, agradeço a todos os meus amigos de graduação que me acompanharam diariamente, mesmo nas atuais circunstâncias de

isolamento social, durante a confecção deste trabalho. Obrigada Amanda, Carol, Denise, Felipe, Iure, Luna e Uliana por toda a amizade, apoio e momentos compartilhados, bons e ruins. Obrigada por sempre suportarem meus surtos de desespero e sempre me motivarem a não desistir. Estou com saudades, pessoal.

"É preciso se erguer acima das discordâncias
e do caos e continuar acreditando."
(Hera)

Resumo

Na literatura, existem estudos de confiabilidade de sistemas de potência com diversas resoluções de perfis de operação. Perfis de operação de altas resoluções, apesar de representarem mais precisamente o comportamento real das condições de operação do sistema, são mais difíceis de serem registrados corretamente e acarretam simulações de vida útil com elevado esforço computacional. Perfis de operação de baixas resoluções são uma alternativa interessante para solucionar esses problemas. Porém, trabalhos anteriores demonstram que a diminuição da resolução dos perfis de operação modifica a dinâmica do perfil de operação real, o que inevitavelmente afeta a precisão das previsões de desgaste de conversores eletrônicos. Em vista destes pontos, este trabalho propõe uma estratégia de correção para reduzir os erros nas estimativas de consumo de vida útil de um inversor fotovoltaico (FV) monofásico conectado à rede elétrica causados pela diminuição da resolução dos perfis de operação. A principal ideia da estratégia é determinar uma equação de correção que seja capaz de reduzir os desvios nas estimativas de consumo de vida útil de um inversor FV específico quando perfis de operação com diferentes valores de tempo de amostragem são utilizados no procedimento de avaliação de vida útil. Neste trabalho, um estudo sobre os efeitos do tempo de amostragem do perfil de operação nos resultados de consumo de vida útil de dispositivos semicondutores de potência e capacitores eletrolíticos de um inversor FV monofásico é realizado. Em seguida, uma equação para corrigir os resultados de consumo de vida útil dos transistores bipolares de porta isolada do estágio cc/ca de um inversor FV de 5 kW, considerando o estresse térmico causado pela frequência da rede, é determinada baseada em perfis de operação das cidades de Aalborg (Dinamarca) e Petrolina (Brasil). A metodologia proposta é validada aplicando a equação de correção determinada a três perfis de operação de diferentes localidades. Os resultados mostram que a equação de correção determinada pela estratégia proposta melhora as avaliações de vida útil para os perfis de operação de baixas resoluções considerados. Além disso, a equação determinada mostrou-se adaptável às características de irradiância solar e temperatura ambiente de diferentes regiões do mundo.

Palavras-chaves: Inversor fotovoltaico, previsão de desgaste, resolução do perfil de operação, melhoria da avaliação de vida útil.

Abstract

In literature, there are reliability studies in electrical power systems with several mission profile (MP) resolutions. High-resolutions MPs, although more accurately represent the actual behavior of the system operating conditions, are more difficult to be correctly recorded and lead to lifetime simulations with high computational burden. Low-resolutions MPs are an interesting alternative to solve these issues. However, previous works demonstrate that the decreasing of the MP resolution modifies the dynamics of the actual mission profile, which inevitably affects the wear-out predictions accuracy of power converters. In view of these points, this work proposes a correction strategy to reduce the errors in the lifetime consumption (LC) estimations of a single-phase grid-connected photovoltaic (PV) inverter due to the MP resolution decreasing. The strategy main idea is to determine a correction equation which is able to reduce the deviations in the LC estimations of a specific PV inverter when MPs with different sampling time values are used in the lifetime evaluation procedure. In this work, a study about the MP sampling time effects on the LC results of power semiconductor devices and electrolytic capacitors of a single-phase PV inverter is performed. Then, an equation to correct the LC results of the dc/ac stage insulated gate bipolar transistors of a 5 kW PV inverter, considering the short-cycle thermal loading, is determined based on MPs from the cities of Aalborg (Denmark) and Petrolina (Brazil). The proposed methodology is validated by applying the determined correction equation to three MPs from different locations. The results show that the correction equation determined by the proposed strategy improves the lifetime evaluations for the considered low-resolutions MPs. In addition, the determined equation proved to be adaptable to the characteristics of solar irradiance and ambient temperature of different regions of the world.

Key-words: Photovoltaic inverter, wear-out prediction, mission profile resolution, lifetime evaluation improvement.

List of Figures

List of Tables

List of abbreviations and acronyms

ac	Alternating Current
dc	Direct Current
ESR	Equivalent Series Resistance
FV	*Fotovoltaico*
IEEE	Institute of Electrical and Electronics Engineers
IGBT	Insulated Gate Bipolar Transistor
LC	Lifetime Consumption
LCL	Inductance Capacitance Inductance
MMC	Modular Multilevel Converter
MP	Mission Profile
MPPT	Maximum Power Point Tracking
P&O	Perturb and Observe
PI	Proportional Integral
PQ	Active and Reactive Power
PR	Proportional Resonant
PV	Photovoltaic
PWM	Pulse Width Modulation
RMS	Root Mean Square
SOGI-PLL	Second Order Generalized Integrator Phase-Locked Loop
TDK	Tokyo Denki Kagaku

List of symbols

a_1	$s(T_s)$ fitting coefficient
a_2	$s(T_s)$ fitting coefficient
a_3	$s(T_s)$ fitting coefficient
a_4	$s(T_s)$ fitting coefficient
A	Semiconductor technology factor
ar	Semiconductor bond wire aspect ratio
C	Semiconductor lifetime model fitting coefficient
C_{dc}	Dc-link capacitance
C_f	LCL filter capacitance
C_{pv}	Boost input capacitance
E_a	Activation energy
$Error(T_s)$	Aalborg MP average error curve
F	Correction factor
f_d	Diode related constant used in semiconductor lifetime model
f_i	Operation frequency
f_n	Grid fundamental frequency
G	Solar irradiance
G_{avg}	Solar irradiance MP average
$G_{avg,AAL}$	Solar irradiance average of the Aalborg MP
$G_{avg,PTR}$	Solar irradiance average of the Petrolina MP
i	Harmonic order
i_b	Boost converter current
i_b^*	Boost converter current reference

$I_{i(RMS)}$	RMS value of capacitor current harmonic components
i_{pv}	Photovoltaic array output current
i_s	Full-bridge output current
i_s^*	Full-bridge output current reference
k_b	Boltzmann constant
L	Time to failure
L_0	Capacitor nominal lifetime
L_b	Boost converter inductance
L_f	LCL filter inductance (inverter side)
L_g	LCL filter inductance (grid side)
$LC^{'}$	LC value estimated to calculate F
$LC^{'}_{AAL}$	Aalborg MP LC value estimated to calculate F
$LC^{'}_{PTR}$	Petrolina MP LC value estimated to calculate F
$LC_{calibrated}$	Corrected and calibrated LC values
$LC_{corrected}$	Corrected LC values
$LC_{(long)}$	Long-cycles LC
$LC_{(short)}$	Short-cycles LC
limit_{lower}	Spread lower limit
limit_{upper}	Spread upper limit
N_f	Number of cycles to failure
$N_f^{'}$	N_f value estimated to calculate F
$N^{'}_{f,AAL}$	Aalborg MP N_f value estimated to calculate F
$N^{'}_{f,PTR}$	Pterolina MP N_f value estimated to calculate F
$N_{f,long}$	Long-cycles N_f
$N_{f,short}$	Short-cycles N_f
MP_1	Mission profile decimated considering the first point of the original MP as the start point for the decimation process

MP_2	Mission profile decimated considering the second point of the original MP as the start point for the decimation process
P^*	Active power reference
$P_{c,loss}$	Capacitor power losses
P_{dc}	Dc-link instantaneous power
P_{pv}	Photovoltaic array output active power
Q^*	Reactive power reference
R_b	Boost converter internal resistance
R_c	Equivalent thermal resistance
$R_{c,dc}$	Dc-link capacitor thermal resistance
$R_{c,pv}$	Boost input capacitor thermal resistance
R_d	LCL filter damping resistance
R_f	LCL filter internal resistance (inverter side)
R_g	LCL filter internal resistance (grid side)
R_{ha}	Heatsink thermal resistance
$R_{jc,d}$	Diode junction-case thermal resistance
$R_{jc,i}$	IGBT junction-case thermal resistance
$s_{avg}(T_s)$	Arithmetic average of the upper and lower limits of the spread
S_n	PV inverter rated power
$s(T_s)$	Fitted $s_{avg}(T_s)$
T_0	Capacitor nominal temperature
T_{amb}	Ambient temperature
T_{avg}	Ambient temperature MP average
$\mathrm{T}_{avg,AAL}$	Ambient temperature average of the Aalborg MP
$\mathrm{T}_{avg,PTR}$	Ambient temperature average of the Petrolina MP
T_h	Hot-spot temperature

T_j	Junction temperature
T_{jm}	Mean junction temperature
t_{on}	Heating time
T_{pv}	Photovoltaic panels temperature
T_s	Mission profile sampling time
$T_s^{'}$	Mission profile sampling time for decimation process
V_0	Capacitor nominal operating voltage
V_c	Capacitor operating voltage
v_{dc}	Dc-link voltage
v_{dc}^*	Dc-link voltage reference
v_g	Grid voltage
v_{pv}	Photovoltaic array output voltage
v_{pv}^*	Photovoltaic array output voltage reference
v_α	Grid voltage in stationary reference frame
v_β	Grid voltage in stationary reference frame
α	Semiconductor lifetime model fitting coefficient
β_0	Semiconductor lifetime model fitting coefficient
β_1	Semiconductor lifetime model fitting coefficient
ΔT_j	Junction temperature fluctuation
γ	Semiconductor lifetime model fitting coefficient

Contents

1 Introduction

The majority of the electricity consumed in the world is generated from non-renewable resources. At the end of 2019, for example, approximately 73% of the global energy production was generated from fossil fuels, as natural gas, coal and oil (REN 21, 2020). However, the environmental degradation, socioeconomic impacts and depletion of fossil fuels have driven the world to increasingly invest in the use of renewable energy sources (Guangul; Chala, 2019). As reported in (REN 21, 2020), renewable energies have continuously dominated the net annual additions in the global power generating capacity since 2015, surpassing the net additions of fossil fuels and nuclear power combined.

Among the available renewable sources, solar photovoltaic (PV) has highlighted for its expressive growth in recent years. In 2019, more than 200 GW of new renewable power generating capacity were installed worldwide, being around 115 GW of contribution from PV energy (REN 21, 2020). Such additions led PV generation to reach the mark of 627 GW of global capacity and to occupy the position of third largest renewable electricity technology, behind only of hydropower and wind power plants (REN 21, 2020; IEA, 2020). Furthermore, forecasts also indicate strong expansion trends for the solar PV technology. International Energy Agency predicts an increase in renewable power capacity by 1200 GW until 2024, being 60% of this increasing generated only by the solar PV production (IEA, 2019).

Nonetheless, although the aforementioned statistics indicate a positive trend towards the diversification of the world energy matrix, the increasing and accelerated penetration of PV systems connected into the grid have raised concerns related to the reliability of these systems. Unexpected failures during PV systems operation (and in power electronic systems in general) cause downtime events and unscheduled expenses with maintenance or replacement, which consequently increase the produced PV energy final cost (Yang; Sangwongwanich; Blaabjerg, 2016). In addition, such failures negatively affect the reputation of the devices manufacturers and the customers satisfaction (Pahwa; Rahman, 2017). For these reasons, the analysis of PV systems reliability became an important target of study for many researchers in the area.

The PV energy is injected into the grid by the use of a PV inverter, a device responsible to convert the direct current (dc) produced by the PV panels in alternating current (ac). According to field experiments, this inverter is pointed out as the main cause of failures in PV systems. In (Golnas, 2013), an analysis of more than 3500 failure tickets issued for 350 PV systems over a period of 27 months was performed. The results demonstrated that 43% of the failures occurred in the monitored systems were caused

by the inverter. In (IEA, 2002), a study performed with 2056 grid-connected PV systems showed that about 65% of the failures founded in the analyzed systems were motivated by faults in the inverter. Industrial surveys still show that power semiconductor devices and electrolytic capacitors are the most critical components in PV inverters and in power electronics systems in general (Yang et al., 2011; Falck et al., 2018).

In recent years, reliability evaluation methodologies have been increasingly employed in PV inverters to ensure that more reliable equipments are designed (Cupertino et al., 2019; Sangwongwanich et al., 2020). Different approaches to precisely estimate the lifetime of electronic systems are still consistently developed and proposed in literature (Wang; Wang; Zhang, 2020). In many of the approaches, the solar irradiance and ambient temperature operating conditions (in which the PV inverter is subjected) are normally considered during the lifetime prediction procedure. The consideration of such conditions, referred here as mission profile (MP), allows that more realistic and accurate reliability assessments to be obtained. This is because the mission profile of a PV inverter strongly affects the PV power production and, consequently, the thermal loading and the system components lifetime (De León-Aldaco et al., 2013; Sintamarean et al., 2014).

1.1 Motivation and Problematic

In literature, there are power converters reliability studies with several mission profile resolutions. Table 1 summarizes some MP resolutions which were adopted in previous works to predict the lifetime of power semiconductor devices and capacitors. In this table, T_s refers to the MP sampling time, i.e., the time interval in which the mission profile data were measured and recorded.

Although high-resolution mission profiles represent more accurately the actual behavior of the operating conditions of a power converter, the lifetime simulations performed with such profiles consume considerable computational processing time. This is due to the fact that high-resolution MPs have a large number of data points to be accounted in the reliability analysis (Sangwongwanich; Wang; Blaabjerg, 2020). In addition, high-resolution MPs are harder to correctly record. In this context, the use of low-resolution mission profiles becomes an interesting solution, as long as there is no generality loss in the results.

However, previous studies show that there is a straightforward connection between the MP resolution and the estimated results for the lifetime consumption (LC) of power systems. These works demonstrate that the decreasing of the MP resolution modifies the dynamics of the actual mission profile, which inevitably affects the wear-out prediction accuracy of power systems (Zhang et al., 2017b; Zhang et al., 2017a; Sangwongwanich et al., 2018; Vernica; Wang; Blaabjerg, 2018; Silva et al., 2020).

Table 1 – Mission profiles sampling times in literature.

Sampling time T_s	Power semiconductor devices	Capacitors
$<$ 1 min	(Yang; Wang; Blaabjerg, 2014) (Reigosa et al., 2016) (Dbeiss; Avenas; Zara, 2017) (Callegari et al., 2019)	-
1 min	(Sintamarean et al., 2014) (Cupertino et al., 2019) (Gatla et al., 2019)	(Lenz; Pinheiro; Sartori, 2017) (Cupertino et al., 2019)
5 min	(Anurag; Yang; Blaabjerg, 2015) (Yang; Sangwongwanich; Blaabjerg, 2016) (Zare et al., 2017) (Sangwongwanich et al., 2018) (Bouguerra et al., 2020)	(Zare et al., 2017) (Sangwongwanich et al., 2018)
10 min	(De León-Aldaco; Calleja; Aguayo Alquicira, 2015)	-
1 h	(Liu et al., 2014) (Zhou; Blaabjerg, 2020)	(Zhou; Blaabjerg, 2020)

In (Sangwongwanich et al., 2018), the effects of the MP resolution on the reliability analysis of power semiconductor devices of a single-phase PV inverter are investigated. The results show that the accumulated damage of the evaluated devices are reduced by 50% when the MP sampling time increases from 1 s to 5 min. In (Vernica; Wang; Blaabjerg, 2018), a similar investigation is developed, extending the reliability analysis to dc-link capacitors of a three-phase PV system. This work concludes that different accumulated damages and lifetime predictions can be found for the PV inverter components depending on the adopted MP sampling time. The results show that the PV system lifetime estimated considering a MP with sampling time equal to 1 min is approximately 30% lower than the lifetime estimated for a MP with sampling time equal to 1 h.

References (Zhang et al., 2017b; Zhang et al., 2017a) demonstrate that the same effects previously described are verified in wind turbines. Reference (Zhang et al., 2017b) evaluates the reliability of Insulated Gate Bipolar Transistor (IGBT) modules used in a Modular Multilevel Converter (MMC) considering MPs with sampling times equal to 1 s, 10 min and 1 h. The conclusions show that the 10 min and 1 h mission profiles result in underestimation of the MMC annual lifetime consumption, which means that the MMC lifetime is overestimated. In (Zhang et al., 2017a), three mission profiles with different lengths and resolutions are explored. The study is realized considering the lifetime evaluation of a doubly-fed induction generator power converter. The results demonstrate that the lifetime estimated for the converter power devices reduces when the MP resolution increases.

Nonetheless, although the effects of the MP resolution decreasing on the wear-out prediction accuracy of power systems are known, no solution was proposed to avoid or reduce these issues. This means that there are errors in the LC estimated results when low-resolution MPs are used in the PV inverter lifetime evaluation.

1.2 Contributions and Objectives

This work proposes a correction strategy to reduce the errors in the LC estimations of a single-phase grid-connected PV inverter due to the MP resolution decreasing. The strategy main idea is to determine a correction equation which is able to reduce the errors in the LC estimations of a specific PV inverter, when MPs with different sampling time values are used in the lifetime evaluation procedure. Thus, even in situations where there are no high-resolution MPs, the correction equation can be used to minimize the deviations which will naturally be found in the estimated LC results with the available MPs. Besides, the proposed strategy is developed to find a correction equation applicable to any region of the world. In this sense, the correction equation is adaptable to the characteristics of solar irradiance (G) and ambient temperature (T_{amb}) of the considered location. In summary,

this work provides the following contributions:

- Proposing a methodology to determine a correction equation which is able to reduce the errors in the *LC* estimations of a specific PV inverter caused by the MP resolution decreasing;
- Offering an alternative to obtain *LC* estimations without significant deviations using low-resolution mission profiles;
- Determination of a correction equation adaptable to the characteristics of solar irradiance and ambient temperature of different regions of the world;
- Possibility to replicate the proposed methodology for different PV inverter technologies.

The results produced in this work originated the following journal paper:

1. R.P. Silva, R.C. de Barros, E.M.S. Brito, W.C. Boaventura, A.F. Cupertino, and H.A. Pereira, "Pursuing computationally efficient wear-out prediction of PV inverters: The role of the mission profile resolution," in Microelectronics Reliability, vol. 110, 2020. Available: http://www.sciencedirect.com/science/article/pii/S0026271419311746.

A second paper derived from this work is in finalization process and is titled as:

2. "Correction Strategy for Wear-out Prediction of PV Inverters Considering the Mission Profile Resolution Effects".

The author also contributed to the following conference article in the topic of PV inverters lifetime evaluation:

1. R. C. de Barros, R. P. Silva, D. B. da Silveira, W. C. Boaventura, A. F. Cupertino and H. A. Pereira, "Third Harmonic Injection Method for Reliability Improvement of Single-Phase PV Inverters," 2019 IEEE 15th Brazilian Power Electronics Conference and 5th IEEE Southern Power Electronics Conference (COBEP/SPEC), Santos, Brazil, 2019, pp. 1-6. Available: https://ieeexplore.ieee.org/document/9065858.

A second paper in this topic was sent to IEEE Transactions on Energy Conversion with the following tittle:

2. "Third-Harmonic Current Injection for Wear-out Reduction in Single-Phase PV Inverters".

1.3 Text Organization

This work is divided in five chapters. This first chapter presented the context, problematic, motivation, objectives and contributions of the present work. Chapter 2 is composed by a brief description of the PV system and the control strategy adopted in this work. The reliability assessment procedures of the PV inverter components are also approached. Chapter 3 describes the process of the mission profile decimation and the effects of the MP resolution in the PV inverter lifetime consumption estimation. Then, a correction strategy to minimize the errors in the inverter LC results caused by the MP resolution decreasing is proposed. Chapter 4 presents the case study, exposing the mission profiles employed in this work to validate the proposed correction methodology. The correction results are subsequently presented in Chapter 5. Finally, the conclusions of this work are stated in Chapter 6.

2 Literature Review

In this chapter, the single-phase double-stage PV inverter adopted in this work for the development of the proposed correction methodology is firstly presented. A brief description about the PV system control strategies is also approached. Then, the lifetime evaluation procedures of power semiconductor devices and electrolytic capacitors are described.

2.1 Single-phase Grid-connected PV Inverter

The structure of the single-phase grid-connected PV inverter considered in this work is presented in Fig. 1. The main parameters of the illustrated system are summarized in Table 2. As observed, the PV inverter is composed by two stages. The first stage is a dc/dc stage which consists of a boost converter. The second stage is a dc/ac stage which consists of a full-bridge single-phase inverter composed of four IGBTs with anti-parallel diodes. These power semiconductor devices are rated at 20 A/600 V and manufactured by Infineon under part number IKW20N60T. The input capacitance of the boost converter is composed of two 270 μF/500 V capacitors connected in parallel. Likewise, the dc-link capacitance is composed of three 1000 μF/450 V capacitors connected in parallel. These components are aluminum electrolytic capacitors manufactured by TDK under part number B43522. A LCL filter is used to attenuate the high frequency harmonics components generated by the inverter switching process. In addition, the inverter output is synchronized with the grid through a Second Order Generalized Integrator in cascade with the Phase-Locked Loop (SOGI-PLL) structure (Ciobotaru; Teodorescu; Blaabjerg, 2006).

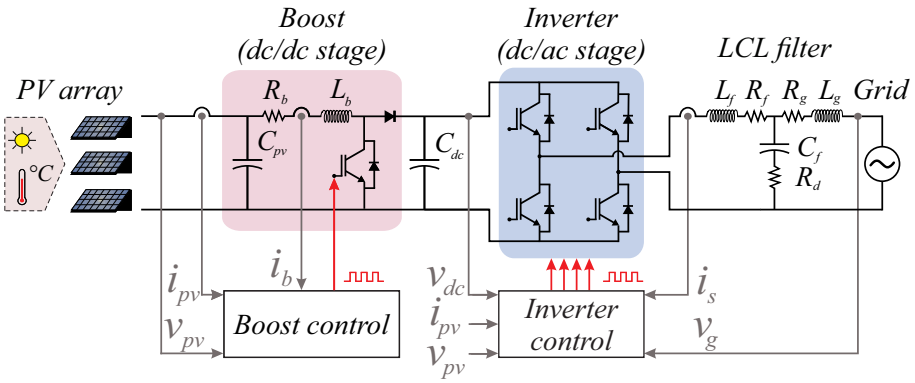

Figure 1 – Structure of a single-phase grid-connected PV inverter.

The control strategy adopted in the dc/dc stage is presented in Fig. 2. The boost converter performs the maximum power point tracking (MPPT) to extract the maximum

Table 2 – Parameters of the single-phase grid-connected PV system.

Parameter	Value
Inverter rated power (S_n)	5 kVA
Grid voltage (v_g)	220 V
Grid fundamental frequency (f_n)	60 Hz
Boost switching frequency	12 kHz
Full-bridge switching frequency	12 kHz
LCL filter inductance ($L_f = L_g$)	2 mH
LCL filter internal resistance ($R_f = R_g$)	0.3 mΩ
LCL filter capacitance (C_f)	0.1 μF
LCL filter damping resistance (R_d)	4 Ω
Dc-link voltage (v_{dc})	400 V
Dc-link capacitance (C_{dc})	3000 μF
Boost input capacitance (C_{pv})	540 μF
Boost converter inductance (L_b)	0.8 mH
Dc-link capacitor thermal resistance ($R_{c,dc}$)	4 K/W
Boost input capacitor thermal resistance ($R_{c,pv}$)	8 K/W
IGBT junction-case thermal resistance ($R_{jc,i}$)	0.9 K/W
Diode junction-case thermal resistance ($R_{jc,d}$)	1.5 K/W
Heatsink thermal resistance (R_{ha})	0.32 K/W

power produced by the PV panels. In this work, MPPT is implemented with the Perturb and Observe (P&O) algorithm (Esram; Chapman, 2007; Sera et al., 2013). Thus, for each operating condition, the voltage reference v_{pv}^* relative to the maximum power point is provided. The control of the solar array output voltage v_{pv} supplies the current reference i_b^* for the control of the boost converter inductor current. The control structure is based on proportional-integral (PI) controllers and the final product is the pulse width modulation (PWM) signal, which is sent to the semiconductor power device of the boost converter. The PI controllers gains are found by pole allocation method, as described in (Xavier, 2018).

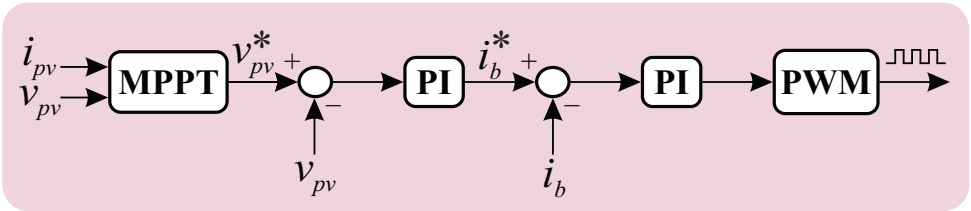

Figure 2 – Control block diagram of the PV converter dc/dc stage.

Fig. 3 shows the control block diagram of the dc/ac stage. This control consists of a outer voltage loop and a inner current loop. The outer loop is responsible to regulate the dc-link voltage and it is based on the v_{dc}^2 method (Yazdani; Iravani, 2010). This control structure uses a conventional PI controller to obtain the dc-link instantaneous power P_{dc}. The controller gains are obtained according to (Xavier, 2018). Then, the active power reference P^* is found from the difference between the PV panel generated power P_{pv} and

P_{dc}. In the inner loop, the current reference i_s^* is calculated through the active power and reactive power (PQ) theory (Saitou; Shimizu, 2002; Yang; Blaabjerg; Zou, 2013). In this case, the reactive power reference is considered zero. The inner loop control is based on a proportional-resonant (PR) controller, which has resonant frequency tuned to the grid fundamental frequency. This controller is implemented according to the observations made in (Yepes et al., 2011). The PR controller output is added to the grid voltage feed forward signal v_g and the PWM signal intended for the semiconductor devices of the inverter stage are generated. The SOGI-PLL structure provides the grid voltages at the fundamental frequency in stationary reference frame, v_α and v_β, which are required for the i_s^* calculation.

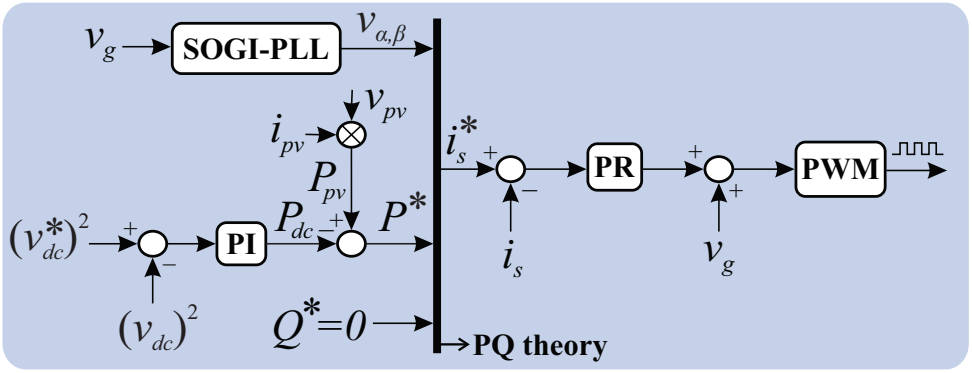

Figure 3 – Control block diagram of the PV converter dc/ac stage.

2.2 Mission Profile Based Lifetime Evaluation

The solar irradiance and ambient temperature operating conditions strongly influence the thermal stress caused to the components of a PV inverter. This thermal stress is considered the main failure mechanisms of electrolytic capacitors and power semiconductor devices, which are the most critical components to failure of a power systems in general (Yang et al., 2011; Oh et al., 2015; Sangwongwanich et al., 2018). Therefore, the lifetime evaluation procedures used in this work take into account the mission profiles influence. Besides, both semiconductor devices and capacitors are considered in this work. The following sections describe the methodologies used to evaluate the lifetime of power semiconductor devices and capacitors.

2.2.1 Lifetime Evaluation of Power Semiconductor Devices

The fluctuations in the PV power production, caused by the mission profile variations, inevitably affect the behavior of the junction temperature T_j of the PV inverter power semiconductor devices. The T_j variations lead the power devices to failure after a certain number of thermal cycles, being the main responsible for wear-out failures in these

devices. Therefore, for the semiconductor devices lifetime evaluation, the mission profile must be translated into thermal loading (Sangwongwanich et al., 2018). Figure 4 shows the main steps of the power devices lifetime evaluation procedure. In order to translate the mission profiles into thermal loading, a power losses look-up table is created considering a defined set of operating conditions. This look-up table has as input parameters the solar irradiance, the PV panels temperature T_{pv} (which can be related to the ambient temperature by the Ross' expression (OLUKAN; EMZIANE, 2014)) and the feedback junction temperature of the components. As a result, the total power losses dissipated in the power devices for each point of the considered mission profile are computed.

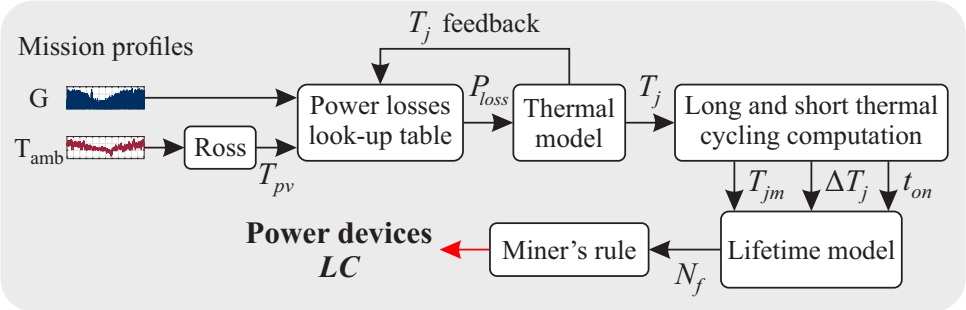

Figure 4 – Lifetime evaluation procedure for power semiconductor devices.

With the total power losses estimated from the mission profiles, the semiconductor devices T_j values are extracted through thermal equivalent circuit models. There are several circuit models which describe the thermal behavior of semiconductor devices. In this work, the used circuit consists of an electro-thermal hybrid model, proposed by (Ma et al., 2015). This model combines the advantages of the Foster and Cauer models, thus ensuring that better T_j estimations are obtained (Ma et al., 2015).

The knowledge of the T_j values allows to obtain information about the thermal cycling of semiconductor devices, such as mean junction temperature T_{jm}, junction temperature fluctuation ΔT_j and heating time t_{on}. These parameters are usually required as input parameters in lifetime models of the semiconductor components. Nonetheless, it is important to remark that the thermal cycling of power devices can be classified mainly in two different terms: long and short thermal cycling. The long-cycles are related to the thermal stress caused by the mission profile variations. The short-cycles are related to the thermal stress caused by the grid frequency (Ma; Blaabjerg, 2012). Therefore, in the dc/dc stage, the power devices are subjected only to long-cycles, while the dc/ac stage devices are subjected to both long and short-cycles. For each of these thermal cycling, the information of T_{jm}, ΔT_j and t_{on} are obtained through different methodologies.

In the long-cycle analysis, the thermal cycling presents an irregular and unpredictable behavior due to the mission profile dynamics. Thus, the rainflow counting algorithm is employed to find thermal cycles with T_{jm}, ΔT_j and t_{on} (Ma; Blaabjerg, 2012). On the

other hand, in the short-cycle analysis, the cycles are already well-defined due to the grid frequency. Therefore, T_{jm} is considered equal to the T_j obtained from the thermal model, t_{on} is equal to half of the grid period and ΔT_j is analytically defined according to the model presented in (Ma; Blaabjerg, 2012). In both described approaches, the number of cycles to failure N_f of the power semiconductor devices is estimated through the following lifetime model, proposed by (Scheuermann; Schmidt; Newman, 2014):

$$N_f = A(\Delta T_j)^{\alpha}(ar)^{\beta_1 \Delta T_j + \beta_0} \left[\frac{C + (t_{on})^{\gamma}}{C+1}\right] e^{\left(\frac{E_a}{k_b T_{jm}}\right)} f_d. \tag{2.1}$$

In Eq. 2.1, the meaning, values and valid ranges of the parameters A, α, β_1, β_0, C, γ, E_a and f_d are defined in (Scheuermann; Schmidt; Newman, 2014). k_b is the Boltzmann constant and ar equal to 0.35 is used in this work. Besides, as explained by (Scheuermann; Schmidt; Newman, 2014), the parameter f_d is equal to 1 to calculate the N_f of IGBTs. For the diodes, f_d equal to 0.6204 must be used.

Finally, the power devices lifetime consumption LC can be computed by using the Miner's rule, represented as follows (Sangwongwanich et al., 2018):

$$LC = \sum_k \left(\frac{1}{N_{f,long_{(k)}}} + \frac{T_s \times f_n}{N_{f,short_{(k)}}} \right), \tag{2.2}$$

where T_s is the mission profile sampling time and f_n is the grid fundamental frequency. $N_{f,long}$ and $N_{f,short}$ are the number of cycles to failure estimated for the long and short-cycles, respectively. As observed, the power devices LC is given by a cumulative sum of the damages caused by the long and short-cycles.

2.2.2 Lifetime Evaluation of Electrolytic Capacitors

Regarding electrolytic capacitors, the hot-spot temperature T_h and the operating voltage V_c are considered the critical stressors (Hao Ma; Linguo Wang, 2005; Wang; Blaabjerg, 2014). Figure 5 shows the main steps of the procedure to evaluate the capacitors lifetime.

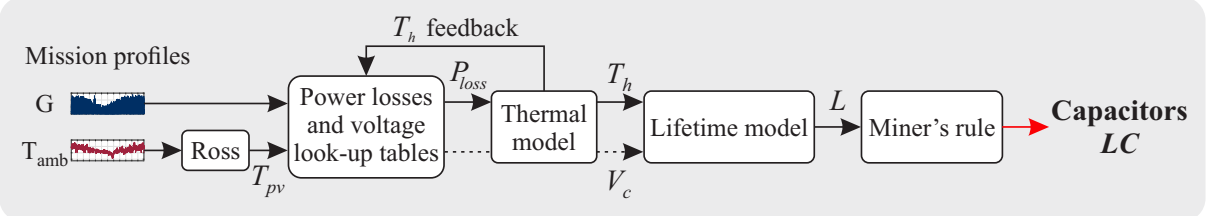

Figure 5 – Lifetime evaluation procedure for electrolytic capacitors.

Firstly, power losses and voltage look-up tables must be created considering a defined set of operating conditions. The capacitor power losses $P_{c,loss}$ are estimated according to the following equation (Lenz; Pinheiro; Sartori, 2017):

$$P_{c,loss} = \sum_i ESR(T_h, f_i) I^2_{i(RMS)}, \tag{2.3}$$

where i is the harmonic order, $I_{i(RMS)}$ is the RMS value of each harmonic component of the capacitor current and ESR is the capacitor equivalent series resistance. As observed, the ESR parameter is directly affected by the hot-spot temperature and the operation frequency f_i (Lenz; Pinheiro; Sartori, 2017).

Then, the generated look-up table, which has as input parameters G, T_{pv} and the feedback T_h, is used to compute the total power losses dissipated in the capacitors for each point of the considered mission profile. With these losses, the capacitor T_h values can be estimated by (Lenz; Pinheiro; Sartori, 2017):

$$T_h = T_{amb} + R_c P_{c,loss}, \tag{2.4}$$

where R_c is the equivalent thermal resistance from hot-spot to ambient. In this work, R_c is equal to 8 K/W for the boost converter capacitor and equal to 4 K/W for the dc-link capacitor (Wang et al., 2019). Then, the time to failure L of capacitors can be obtained through the model given by (Wang; Blaabjerg, 2014):

$$L = L_0 \left(\frac{V_c}{V_0}\right)^{-n} \times 2^{\frac{T_0 - T_h}{10}}, \tag{2.5}$$

where L_0 indicates the capacitor nominal lifetime under the voltage V_0 and the temperature T_0, which are provided in the manufacturers datasheet. V_c is the operating voltage calculated by the voltage look-up table. As the lifetime of aluminum electrolytic capacitors quite depends on the voltage stress level, the value of the voltage stress exponent n equal to 3 is used in this work, as suggested in (Wang; Blaabjerg, 2014). Finally, the capacitor lifetime consumption LC can be determined by the Miner's rule, represented by (Sangwongwanich et al., 2018):

$$LC = \sum_k \left(\frac{T_s}{L_{(k)}}\right), \tag{2.6}$$

where $L_{(k)}$ is the time to failure obtained by 2.5 for a specific sample.

3 Methodology

In this chapter, a strategy to correct the deviations in the *LC* results of a PV inverter when there is a reduction in the MP resolution is proposed. For this end, the decimation process of a MP considering different sampling times is firstly explored. Then, the effects of the MP resolution on the lifetime evaluations of the single-phase double-stage PV inverter components are presented. The display of such results is important to justify some assumptions performed during the development of the proposed correction strategy.

3.1 Mission Profile Decimation Process

Based on a MP sampled with a specific resolution, other profiles with several resolutions can be obtained through the decimation process. This means that a specific MP can be decimated considering different sampling times. This decimation process can occur in different ways. Considering a desired fixed time interval, for example, a given MP can be decimated taking the highest value sample, taking the lowest value sample or calculating the average of the samples which are within the chosen time interval. In this work, the decimation process is performed by selecting one sample of the analyzed MP at each desired fixed time interval. The value of this sample is then kept constant and equal to the selected one until the next sample is taken. This idea is illustrated in Fig. 6, where a specific solar irradiance mission profile of a clear day and a cloudy day is decimated considering three different sampling times. As observed, the mission profile resolution considerably affects the measured profile, especially during a cloudy day.

In Fig. 7, a solar irradiance mission profile with sampling time T_s (Fig. 7(a)) is decimated in a new mission profile with sampling time $T_s^{'}$, which is five times longer than the sampling time of the original MP (Fig. 7(b)). As noted, for every five samples of the original profile, one sample is recorded for the new mission profile. However, as can be observed in the same figure, there is more than one possibility for the decimation process. The detail is in the choice of the start point for the decimation. The profile MP_1, for example, is obtained when the decimation is performed considering the first point of the original MP as the start point for the decimation process. Nonetheless, if the second point of the original MP is used as the start point, the profile MP_2 is created. Following this reasoning, it would be possible to obtain yet another three different MPs with the sampling time $T_s^{'}$.

Although MP_1 and MP_2 have the same sampling time $T_s^{'}$, MP_2 considerably differs from MP_1 and, as a result, different wear-out predictions can be obtained from each of these MPs (Silva et al., 2020). This means that, depending on the start point considered

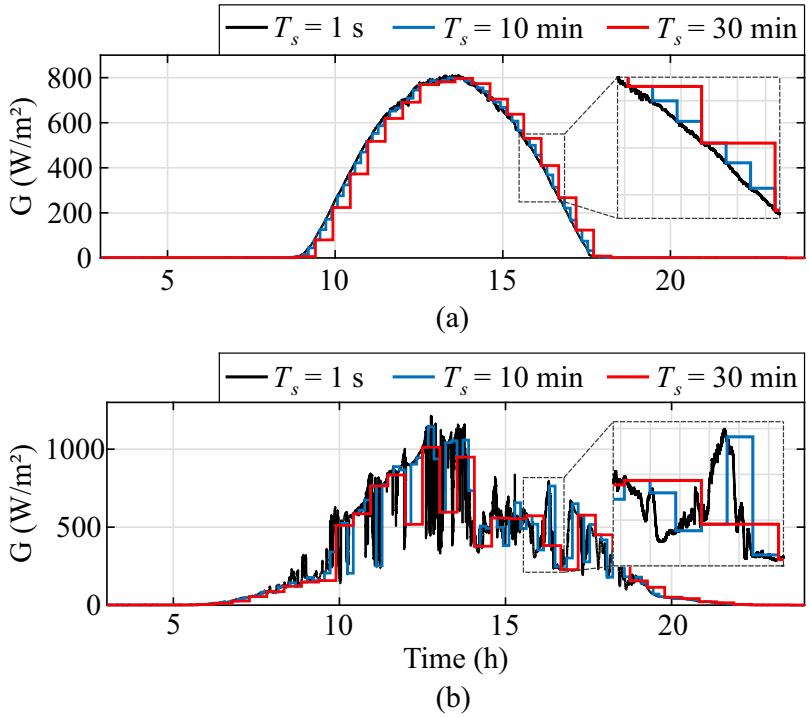

Figure 6 – Solar irradiance profiles with different resolutions during: (a) a clear day and (b) a cloudy day.

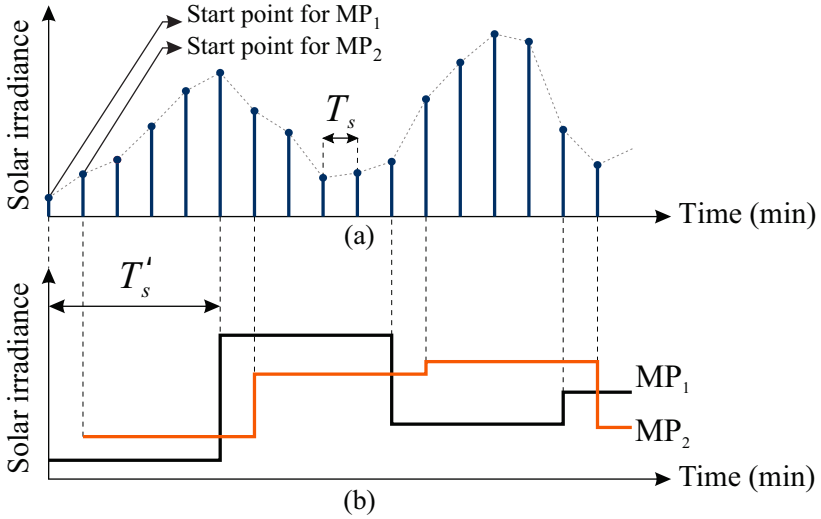

Figure 7 – Mission profile decimation process: (a) original mission profile and (b) two different possibilities for mission profile decimation considering the same sampling time T_s'.

for the sampling of a MP, different LC results can be found for a single MP resolution. Besides, the increasing of the sampling time T_s' also increases the possibilities for the decimation process and, consequently, the amount of LC results which can be obtained for a single MP resolution (Silva et al., 2020).

3.2 Effects of the Mission Profile Resolution on the Lifetime Evaluation of the PV Inverter

To illustrate the effects of the MP resolution and the decimation process on the *LC* results of a PV inverter, the lifetime evaluation methodologies for semiconductor devices and capacitors were carried out considering MPs with different sampling times. The system considered for this analysis was the single-phase double-stage grid-connected PV inverter previously presented in Chapter 2. Besides, the study was performed for the components of the dc/dc and dc/ac stages. Solar irradiance and ambient temperature mission profiles obtained from Aalborg (Denmark) were employed. Such profiles were measured during one year with the sampling time equal to 1 min, as shown in Fig. 8(a)–(b). These MPs correspond to the highest resolution profiles considered in this analysis. Then, these MPs were decimated considering T_s ranging from 1 to 60 min, at 1 min intervals. For each sampling time, the selected point for the sampling start configuration was varied to obtain all possible ways to decimate the mission profiles.

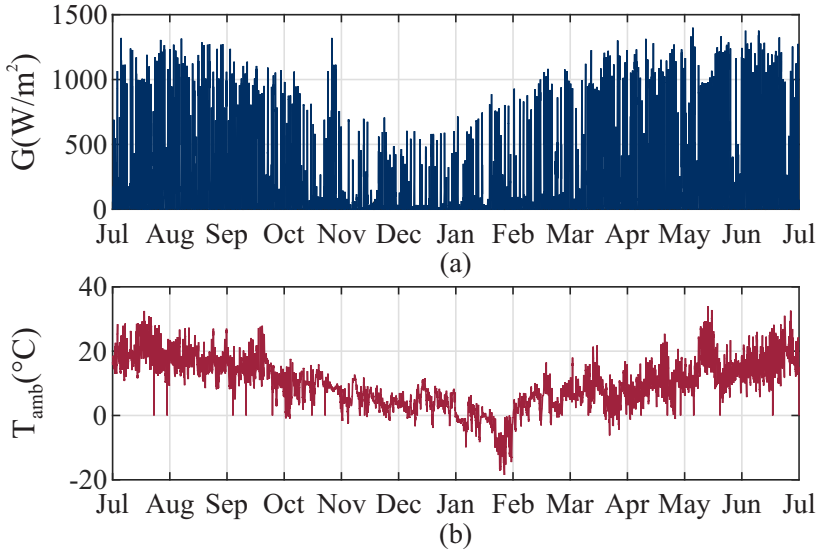

Figure 8 – Aalborg (Denmark) one-year mission profile of: (a) solar irradiance and (b) ambient temperature.

The lifetime consumption of the IGBTs and diodes of the PV inverter are presented in Fig. 9. The results for the short and long-cycles analyzes are presented. The spread corresponds to the maximum and minimum *LC* values which can be found for each MP resolution. Thus, it is observed a *LC* range for each sampling time considered. In addition, to have a better understanding of the process, the *LC* values calculated considering the MP_1 profiles are also displayed. As can be observed, the MP sampling time increasing directly affects the *LC* results of all semiconductor devices. For the IGBT and diode of the boost converter (which are not affected by the thermal stress caused by the grid frequency) and for the long-cycles of the IGBT and diode of the inverter, the *LC* results initially

decrease with the T_s increasing and then, start to increase. However, this behavior does not follow any specific pattern and does not ensure that the results found for high sampling times are accurate. For the short-cycles of the inverter diode, the T_s increasing causes the expansion of the spread around the LC result obtained with the available higher MP resolution. On the other hand, for the short-cycles of the inverter IGBT, all LC results decrease with the T_s increasing.

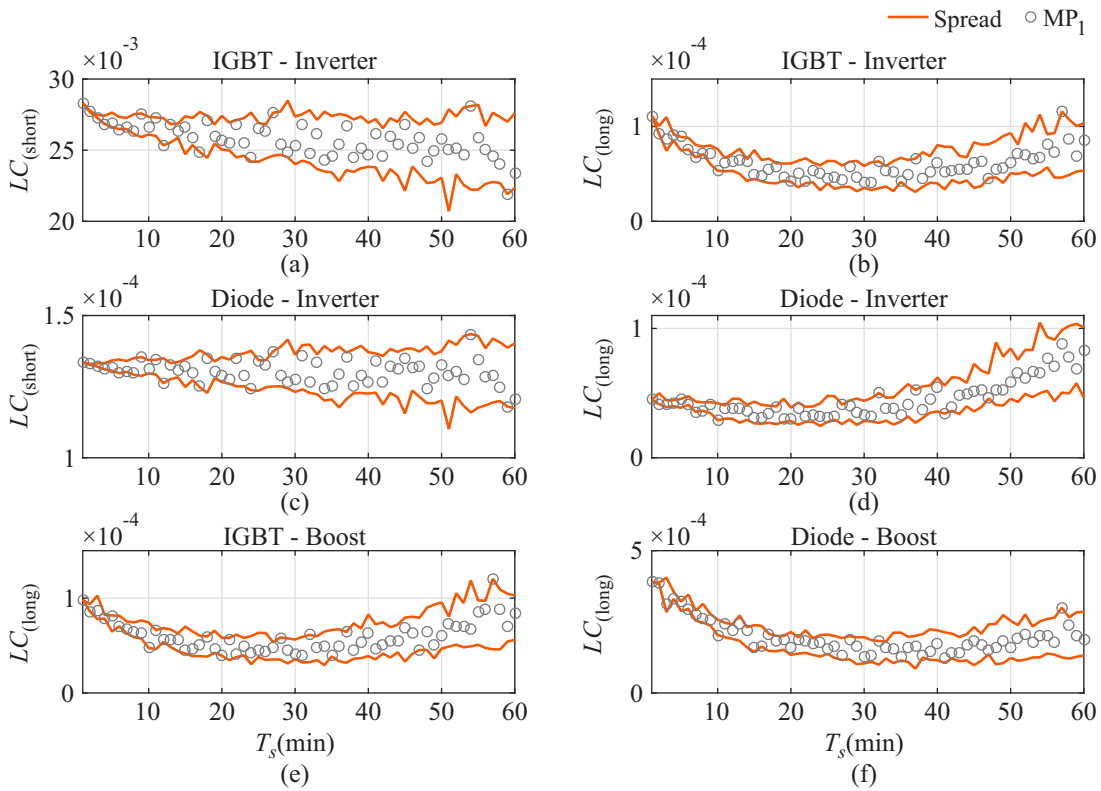

Figure 9 – Lifetime consumption for different T_s values, considering: (a) short-cycle of the inverter IGBT; (b) long-cycle of the inverter IGBT; (c) short-cycle of the inverter diode; (d) long-cycle of the inverter diode; (e) long-cycle of the boost IGBT and (f) long-cycle of the boost diode.

In this context, it is possible to note that, among all the analyzed semiconductor devices, the inverter IGBT is the most stressed component. As observed, the LC values estimated for the short-cycles of the inverter IGBT are considerably higher than the results calculated for the other components, including the LC values estimated for the long-cycles of the own inverter IGBT. Studies developed in (Reigosa et al., 2016; Callegari et al., 2019; Barros, 2019) also show that the damages contribution of the short-cycles are more significant than the contribution of the long-cycles. For this reason, only the inverter IGBT and the short-cycle thermal loading are considered for the development of this work.

The capacitors lifetime consumption of the PV inverter are presented in Fig. 10. The spread and the LC values calculated considering the MP_1 profiles are also displayed. As can be observed, the effects in the lifetime evaluations of the dc-link and boost converter

capacitors due to the MP sampling time increasing are similar. In both cases, the T_s increasing causes the expansion of the spread around the LC result obtained with the available higher MP resolution.

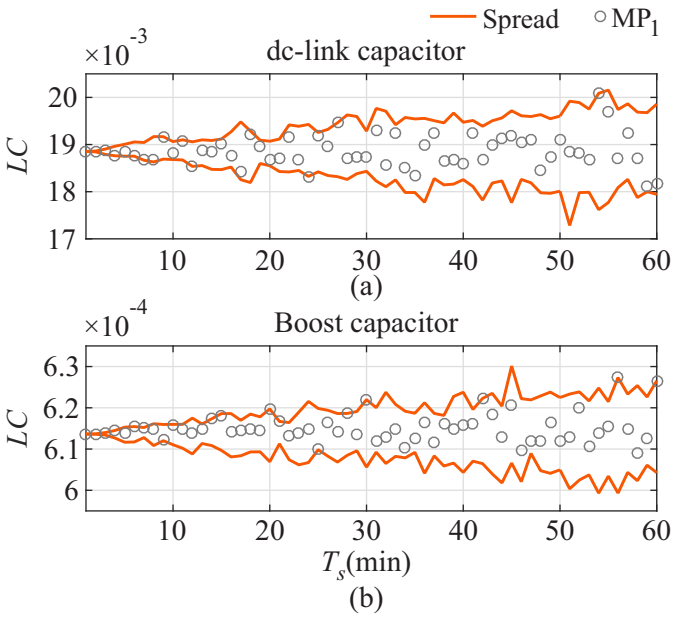

Figure 10 – Lifetime consumption for different T_s values, considering: (a) the dc-link capacitor and (b) the boost converter capacitor.

However, the capacitors are considerably less sensitive to the MP resolution when compared to the inverter IGBTs. Considering the least accurate LC result that can be found when $T_s = 60$ min in relation to the LC value for $T_s = 1$ min, for example, the LC variation of the inverter IGBT in the short-cycles analysis is about 21.05%. On the other hand, for the dc-link and boost capacitors, these results are about 5.36% and 2.12%, respectively. More details about this fact can be found in (Silva et al., 2020). Therefore, the dc-link and boost capacitors are not be considered during the construction of the correction strategy developed in this work.

3.3 Proposed Correction Strategy

In this section, a strategy to correct the LC deviations caused by the MP resolution decreasing is presented and described. The main idea is to provide a way to minimize the errors in the LC estimations after the calculation of such results. Thus, the proposed strategy allows a more accurate reliability analysis of the PV inverter for any available MP resolution.

Fig. 11 shows the first step developed for the elaboration of the proposed correction strategy. The LC results shown in this figure refer to the dc/ac stage IGBTs of the PV inverter stage described in chapter 2 and they were calculated considering the Aalborg

MP previously presented in section 3.2. The LC reference corresponds to the LC result obtained for the highest available Aalborg MP resolution ($T_s = 1$ min). The spread and the LC values calculated considering the MP_1 profile are also shown.

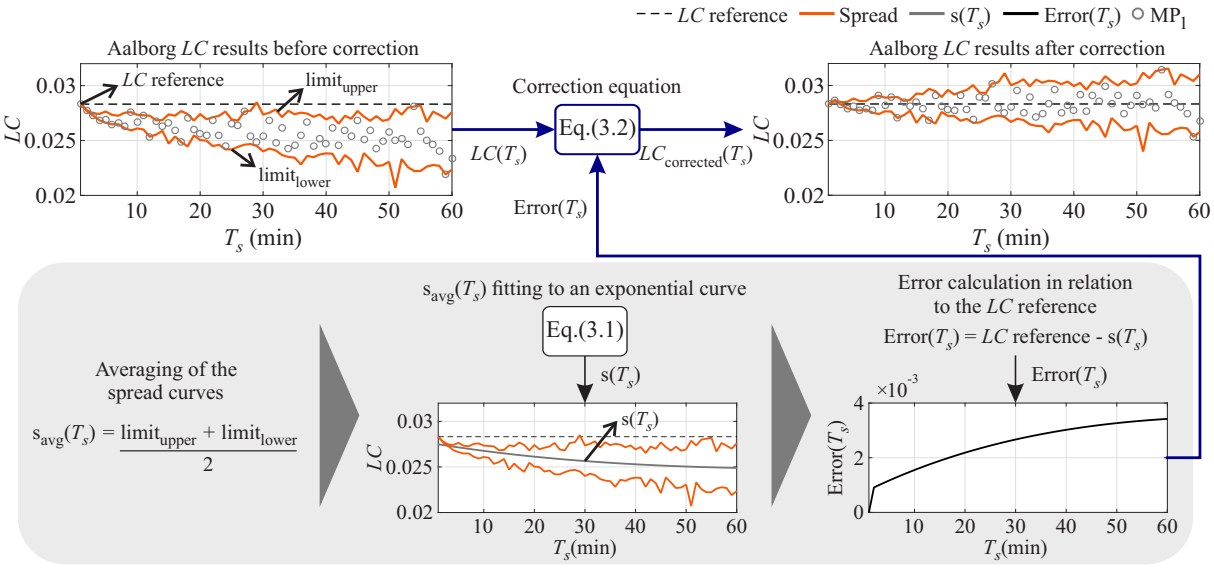

Figure 11 – Proposed correction strategy considering the Aalborg MP.

As can be observed in the LC results before the correction, when T_s increases, the deviations of the LC results in relation to the LC reference, which is 0.0283, also increase. Furthermore, due to the effects of the decimation process, there is a range of possible LC results for each T_s, which represents the spread values.

To correct the effects in the LC results caused by the MP resolution decreasing, the error of each LC result in relation to the LC reference must be determined. However, as there may be a range of LC results for a given T_s, there is also a range of possible errors for each T_s. Thus, in order to find errors which comply with all the results encompassed by the spread, the arithmetic average of the upper limit ($limit_{upper}$) and lower limit ($limit_{lower}$) of the spread $s_{avg}(T_s)$ is firstly calculated. Then, the found average values are fitted to a curve composed of the sum of two exponential terms of the form:

$$s(T_s) = a_1 e^{a_2 T_s} + a_3 e^{a_4 T_s}, \tag{3.1}$$

where a_1, a_2, a_3 and a_4 are adjustable coefficients and equal to 0.0068, -0.0176, 0.0208 and 0.0013, respectively. These values were obtained with the curve fitting tool of the MATLAB software. Subtracting the $s(T_s)$ curve from the LC reference, an average error curve $Error(T_s)$ is estimated. Nonetheless, the error estimated for $T_s = 1$ min is set to zero, since the LC obtained for this sampling time corresponds to the LC reference.

Finally, with $Error(T_s)$ curve, the LC results obtained for the Aalborg MP are

corrected according to the following equation:

$$LC_{corrected}(T_s) = LC(T_s) + Error(T_s). \tag{3.2}$$

As can be observed in the LC results after correction in Fig. 11, the strategy described allows to relocate the spread around the Aalborg MP LC reference, minimizing the deviations originally presented in the LC results. However, it is important to note that the strategy only allows to relocate the spread, which is inherent to the described correction technique.

As the $Error(T_s)$ curve was calculated according to the spread estimated for the Aalborg MP, it is expected that the straight application of Eq. 3.2 in the PV inverter LC results considering MPs from different regions of the world is not able to properly correct the estimated values. To verify this fact, solar irradiance and ambient temperature mission profiles obtained from Petrolina (Brazil) were employed. These data were measured during one year with sampling time T_s equal to 1 min, as shown in Figs. 12(a)–(b).

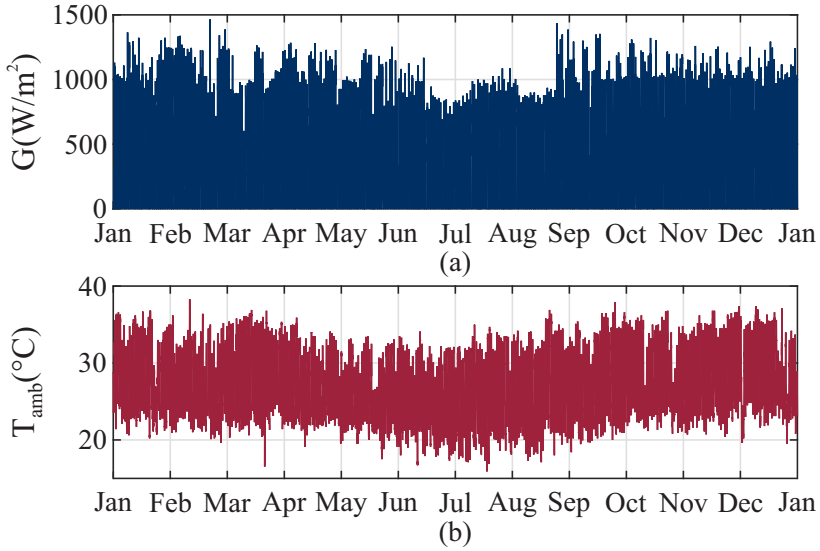

Figure 12 – Petrolina (Brazil) one-year mission profile of: (a) solar irradiance and (b) ambient temperature.

Figs. 13(a)-(b) show, respectively, the LC results estimated for the Petrolina MP before and after the correction represented by the Eq. 3.2. As mentioned, although the proposed correction method minimizes the deviations originally found in the LC results, the results achieved with the correction are not as significant as the results obtained for the Aalborg MP. Nonetheless, the possibility of MPs corrections from any region of the world using the $Error(T_s)$ curve from the Aalborg MP can present strong contributions, since it would not be necessary to obtain the LC references of these other MPs to apply the correction. This means that, even without having MPs sampled at high resolutions, it would still be possible to obtain more accurate LC results. Therefore, a way to adapt

the $Error(T_s)$ curve from the Aalborg MP to MPs from different regions of the world and find a more generic correction equation becomes interesting.

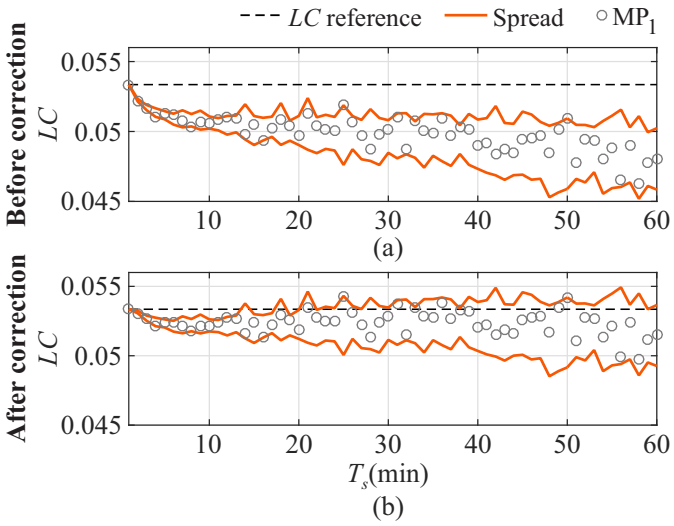

Figure 13 – IGBTs lifetime consumption considering the Petrolina MP: (a) before correction and (b) after the correction considering the Aalborg MP error proposed by 3.2.

To achieve this goal, the $Error(T_s)$ curve must be multiplied by a factor which is able to approximate the Aalborg MP error curve to the error curve necessary to correct the LC values of a specific MP. Thus, the methodology shown in Fig. 14 was developed. This figure shows the procedure used to calculate a correction factor, which is named F in this work. In this case, the mission profile which receives the correction is the Petrolina MP.

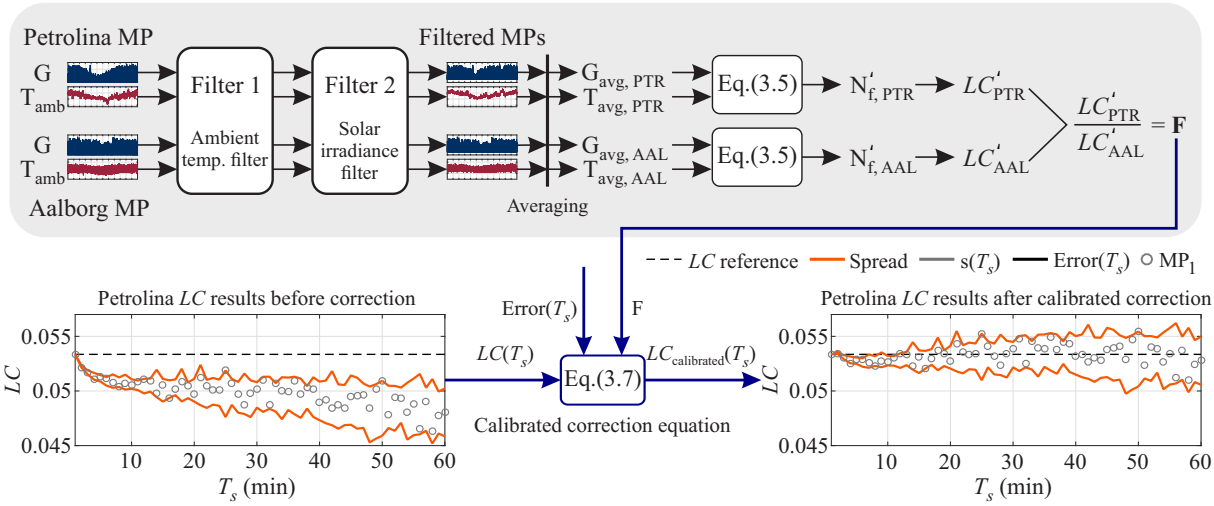

Figure 14 – Correction factor F calculation of the Petrolina MP for the calibration of the correction equation.

To obtain the correction factor F, the Petrolina and Aalborg mission profiles of solar irradiance and ambient temperature are firstly filtered. The purpose of these filtering

is to eliminate the points which least contribute to the lifetime consumption of the PV inverter, such as the points referring to nights (lower irradiance) and winter days (lower temperatures). Filter 1 is responsible to eliminate the lowest ambient temperature points from the profiles. In this filter, the ambient temperature data are placed in ascending order and the temperature which corresponds to a reduction of 8% of the profile data is found. Then, the temperature values lower than the temperature found are filtered. The remaining data are directed to Filter 2. This filter is responsible for eliminating all points with solar irradiance smaller than 200 W/m^2. After the filtering, the arithmetic average of the resulting solar irradiance and ambient temperature mission profiles are calculated. Table 3 shows the averages of solar irradiance G_{avg} and ambient temperature T_{avg} obtained for the Aalborg and Petrolina mission profiles.

Table 3 – Solar irradiance and ambient temperature averages of the Aalborg and Petrolina mission profiles.

MP	G_{avg} (W/m^2)	T_{avg} (°C)
Aalborg	551.0547	15.8441
Petrolina	603.7171	29.3437

The correction factor calculation is performed based on the lifetime model used in this work, previously presented by Eq. 2.1. In this equation, the information regarding the power devices thermal cycling are replaced by relations between the calculated solar irradiance and ambient temperature averages. The solar irradiance and the junction temperature fluctuation ΔT_j are strongly correlated and, for this reason, ΔT_j is replaced by the average of the solar irradiance profile, as presented in Eq. 3.3. In this equation, G_{avg} is divided by 5 to avoid extrapolations in the lifetime model. The mean junction temperature T_{jm}, which can be represented as the sum of the ambient temperature with the value of ΔT_j divided by 2, is replaced by the sum of the average of the ambient temperature profile with G_{avg} divided by 10, as presented in Eq. 3.4.

$$\Delta T_j = \frac{G_{avg}}{5}. \tag{3.3}$$

$$T_{jm} = T_{amb} + \frac{\Delta T_j}{2} = T_{avg} + \frac{G_{avg}}{10}. \tag{3.4}$$

With the replacements of the equations 3.3 and 3.4 in the lifetime model of the Eq. 2.1, the following expression is generated:

$$N_f^{'} = A\left(\frac{G_{avg}}{5}\right)^{\alpha} (ar)^{\beta_1 \frac{G_{avg}}{5} + \beta_0} \left[\frac{C + (t_{on})^{\gamma}}{C+1}\right] e^{\left(\frac{E_a}{k_b (T_{avg} + \frac{G_{avg}}{10})}\right)} f_d. \tag{3.5}$$

Eq. 3.5 is used to estimate a $N_f^{'}$ value for Aalborg and Petrolina mission profiles, individually. With these $N_f^{'}$ values, $LC^{'}$ values for each MP are successively calculated. Finally, with the $LC^{'}$ results, the correction factor F is calculated as the ratio between the $LC^{'}$ of the Petrolina MP and the $LC^{'}$ of the Aalborg MP. Therefore, the correction factor calculation is given by:

$$F = \frac{(\frac{G_{avg,AAL}}{5})^{\alpha}(ar)^{\beta_1 \frac{G_{avg,AAL}}{5}} e^{\left(\frac{E_a}{k_b(T_{avg,AAL}+\frac{G_{avg,AAL}}{10})}\right)}}{(\frac{G_{avg,PTR}}{5})^{\alpha}(ar)^{\beta_1 \frac{G_{avg,PTR}}{5}} e^{\left(\frac{E_a}{k_b(T_{avg,PTR}+\frac{G_{avg,PTR}}{10})}\right)}}, \tag{3.6}$$

where $G_{avg,AAL}$ and $T_{avg,AAL}$ are the solar irradiance and ambient temperature averages of the Aalborg MP, respectively. Likewise, $G_{avg,PTR}$ and $T_{avg,PTR}$ are the solar irradiance and ambient temperature averages of the Petrolina MP, respectively. The obtained correction factor is equal to 1.5920.

However, it was verified that only the multiplication of the $Error(T_s)$ curve by the correction factor F is not enough to approximate the error curve of the Aalborg MP to the error curve necessary to satisfactorily correct the LC results of the Petrolina MP. Thereby, an additional multiplication and a mathematical manipulation was required to calibrate the correction equation given by Eq. 3.2, resulting in:

$$LC_{calibrated}(T_s) = LC(T_s) + [\ln(2.5 \times F) \times Error(T_s)]. \tag{3.7}$$

The LC results for the Petrolina MP before and after the calibrated correction given by Eq. 3.7 are shown in Fig. 14. As observed, the calibrated correction is able to considerably minimize the deviations between the LC reference and the other LC results found for the Petrolina MP.

3.4 Steps for the Implementation of the Proposed Correction Strategy

In summary, the application of the proposed correction methodology in PV inverters equal to the equipment presented in this work requires that the following steps are executed:

- *Step 1*: Filter the lowest temperatures and solar irradiances points of the MP which will receive the correction, as described in section 3.3.
- *Step 2*: After filtering, calculate the ambient temperature and solar irradiance averages of the resulting MP.

- *Step 3*: Replace the ambient temperature and solar irradiance averages in Eq. 3.6, estimating the correction factor F.

- *Step 4*: Replace the F value in the eq. 3.7 and apply the correction to the desired LC result.

On the other hand, in situations where it is desirable to correct the LC results of PV inverter technologies different from the device considered in this work, some steps must first be performed. To replicate the proposed correction methodology, the following steps must be executed:

- *Step 1*: Estimate the PV inverter lifetime consumption based on dc/ac stage IGBTs considering specific solar irradiance and ambient temperature mission profiles. The lifetime evaluation must be performed according to the methodology described in chapter 2, considering the short-cycle thermal loading. In addition, the LC values must be estimated for the original MP, sampled with $T_s = 1$ min, and for MPs obtained through the decimation process considering T_s ranging from 1 to 60 min, at 1 min intervals. In this process, the different start configurations for the MP decimation must be considered. For each T_s, the maximum and minimum LC values, which corresponds to the spread, must be recorded.

- *Step 2*: Calculate the arithmetic average of the upper and lower limits of the spread curves.

- *Step 3*: Fit the obtained average values to an exponential curve represented by Eq. 3.1, thus obtaining the $s(T_s)$ curve.

- *Step 4*: Subtract the $s(T_s)$ curve from the LC reference calculated in Step 1, obtaining the $Error(T_s)$ curve.

- *Step 5*: Choose a new MP to be corrected, different from the one previously used. This MP will be used to find the necessary calibration for the development of the correction equation. Therefore, the Step 1 must also be reproduced for this new MP.

- *Step 6*: Filter the lowest temperatures and solar irradiances points of the reference MP, which is the profile for which the $Error(T_s)$ curve is estimated, and of the other location MP, as described in section 3.3.

- *Step 7*: After filtering, calculate the ambient temperature and solar irradiance averages of the resulting MPs.

- *Step 8*: Replace the ambient temperature and solar irradiance averages in Eq. 3.6, estimating the correction factor F.

- *Step 9*: Multiply the $Error(T_s)$ curve of the reference MP by the correction factor F and add the product obtained to the LC values estimated for the considered mission profile.
- *Step 10*: If the correction is not sufficient or adequate to minimize the LC deviations caused by the T_s increasing, the F factor should be recalibrated.

4 Case Study

The motivation of this chapter is to present the case studies used to validate the proposed correction methodology. For this end, three new and different mission profiles are described. The situations to be analyzed are also addressed.

4.1 Mission Profiles

Three mission profiles from different locations are used to validate the performance of the calibrated correction equation developed in the previous chapter. Figs. 15, 16 and 17 show solar irradiance and ambient temperature data sampled in Goiás (Brazil), Izaña mountain (Tenerife, Spain) and Lindenberg (Germany), respectively. All these data were measured during one year with T_s equal to 1 min.

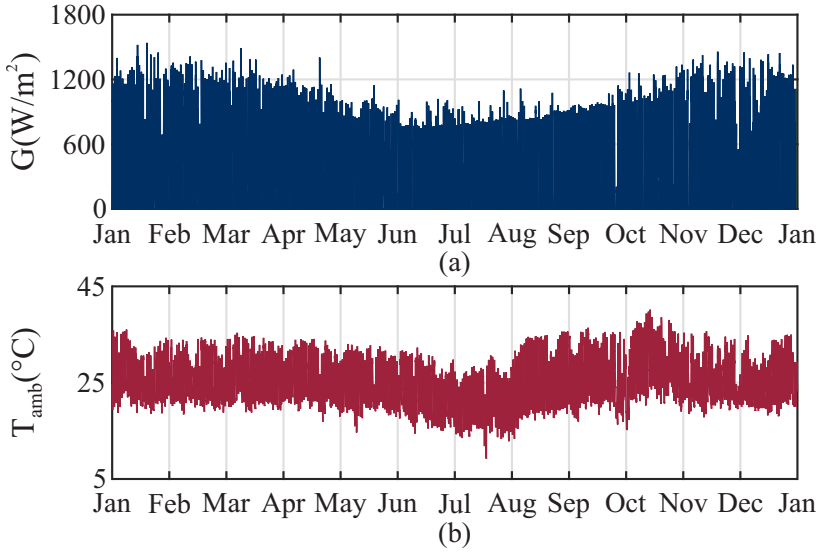

Figure 15 – Goiás (Brazil) one-year mission profile of: (a) solar irradiance and (b) ambient temperature.

For each studied MP, three different situations are analyzed, as follows:

- *Before correction*: In this situation, the *LC* estimations correspond to the values found directly through the lifetime evaluation procedure presented in chapter 2, without any correction technique.

- *After Aalborg correction*: In this case, the *LC* estimations are corrected through Eq. 3.2, using only the error curve generated according to the Aalborg MP.

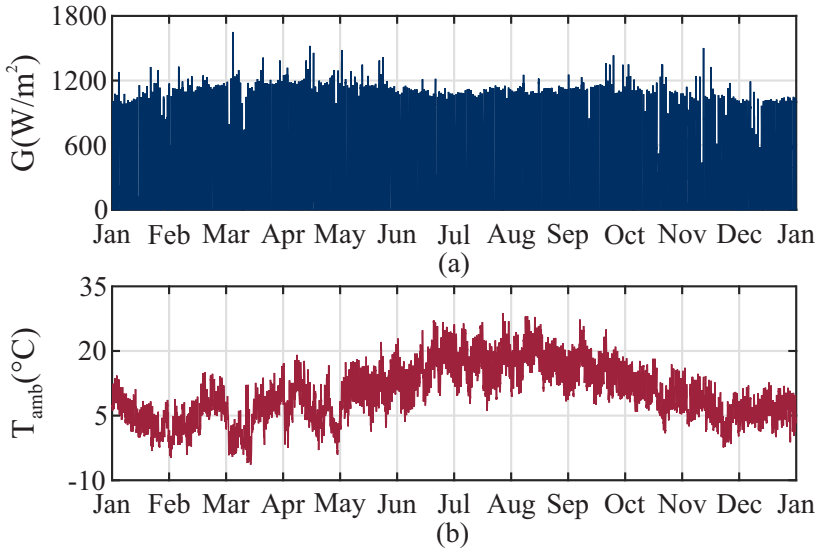

Figure 16 – Izaña mountain (Spain) one-year mission profile of: (a) solar irradiance and (b) ambient temperature.

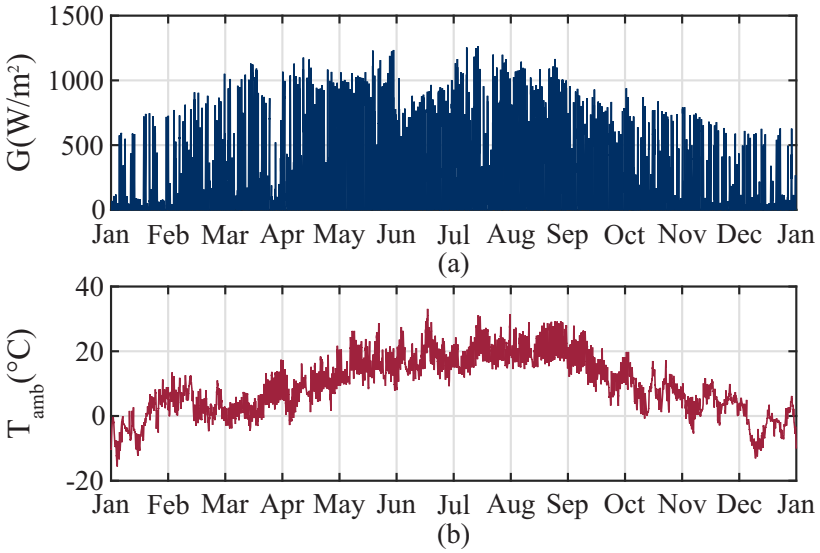

Figure 17 – Lindenberg (Germany) one-year mission profile of: (a) solar irradiance and (b) ambient temperature.

- *After the calibrated correction*: In the third situation, the developed calibrated correction equation, given by Eq. 3.7, is applied to the *LC* results.

The lifetime evaluations are performed considering the single-phase grid-connected PV system previously presented in chapter 2. Moreover, as explained in the methodology, only the IGBTs of the dc/ac stage and the short-cycle thermal loading are considered in the PV inverter lifetime analysis.

5 Results and Discussion

In this chapter, the calibrated correction equation determined by the proposed methodology is applied to the *LC* results estimated considering the mission profiles presented in the previous chapter. The results after the calibrated correction are compared to the original *LC* values to illustrate the advantages of the proposed methodology.

5.1 Calibrated Correction Results

The averages of solar irradiance and ambient temperature of each analyzed MP, required by the proposed methodology, are presented in Table 4. These averages are used to estimate the correction factors F of their respective mission profiles, which are also presented in Table 4. As described in chapter 3, these factors are calculated based on the power devices lifetime model and they are obtained in relation to the Aalborg MP.

Table 4 – Solar irradiance and ambient temperature averages of the Goiás, Izaña and Lindenberg mission profiles and their respective correction factors.

MP	G_{avg} (W/m^2)	T_{avg} (°C)	F
Goiás	604.2619	28.1363	1.5867
Izaña	734.3473	13.3742	3.2061
Lindenberg	503.8469	15.3627	0.6799

For the mission profiles of Goiás, Izaña and Lindenberg, Fig. 18 shows the spread of the possible *LC* results of the PV inverter obtained when the MP sampling time ranges from 1 to 60 min. The results are shown for the situations before correction, after the Aalborg correction and after the calibrated correction. Moreover, the *LC* values estimated considering the profiles MP_1 are displayed.

As observed in Figs. 18 (b) and (e), the Aalborg correction equation approximates the *LC* spread of the Goiás and Izaña mission profiles to its *LC* references, which are 0.0526 and 0.2091, respectively. This means that Eq. 3.2, in these specific cases, already contributes to minimize the effects of the MP resolution decreasing on the *LC* estimations. However, Fig. 18 (h) shows that the Aalborg correction equation leads the *LC* spread of the Lindenberg MP for beyond of its *LC* reference, which is equal to 0.0180. Thus, in this case, the use of the Aalborg correction equation does not contribute for the reduction of the deviations which can be found in the *LC* estimations when low-resolution mission profiles are used.

On the other hand, as shown in Figs. 18 (c), (f) and (i), the calibrated correction equation improves the *LC* results for the three analyzed MPs. For the Goiás and Izaña

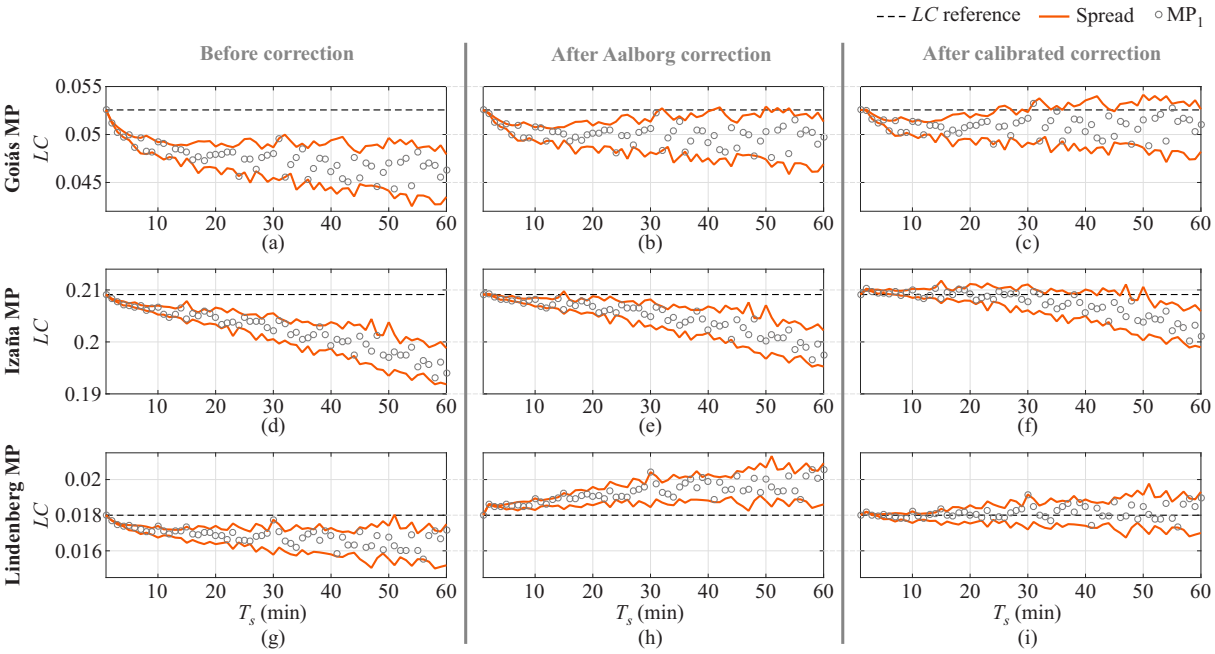

Figure 18 – Lifetime consumption of the PV inverter IGBTs considering the Goiás MP: (a) without correction; (b) with the Aalborg correction equation and (c) with the calibrated correction equation. Lifetime consumption of the PV inverter IGBTs considering the Izaña MP: (d) without correction; (e) with the Aalborg correction equation and (f) with the calibrated correction equation. Lifetime consumption of the PV inverter IGBTs considering the Lindenberg MP: (g) without correction; (h) with the Aalborg correction equation and (i) with the calibrated correction equation.

mission profiles, the calibrated correction equation, when compared to the Aalborg correction equation, enables further approximate the LC spread to its respective references. For the Lindenberg MP, this result is even more significant, since the calibrated correction redistributes the entire LC spread around its LC reference.

Fig. 19 shows how the proposed correction strategy acts on the relocation of the spread of each analyzed MP in relation to the its respective LC references. In this figure, the limits of the spread for the situations without any correction strategy and with the calibrated correction equation are compared. As observed, the developed correction equation approximates the LC spread of each analyzed MP to its respective references, reducing the errors which can be found in the LC estimations when low-resolution MPs are used.

Such results are also quantitatively exhibit in Table 5, where the maximum errors obtained for T_s values equal to 10, 30 and 60 min are compared for each MP. As can be observed, for the three mentioned sampling times and the three studied MPs, the proposed correction strategy achieves significant results in the reduction of the LC errors. For $T_s =$ 10 min, the smallest contribution provided by the calibrated correction equation happens

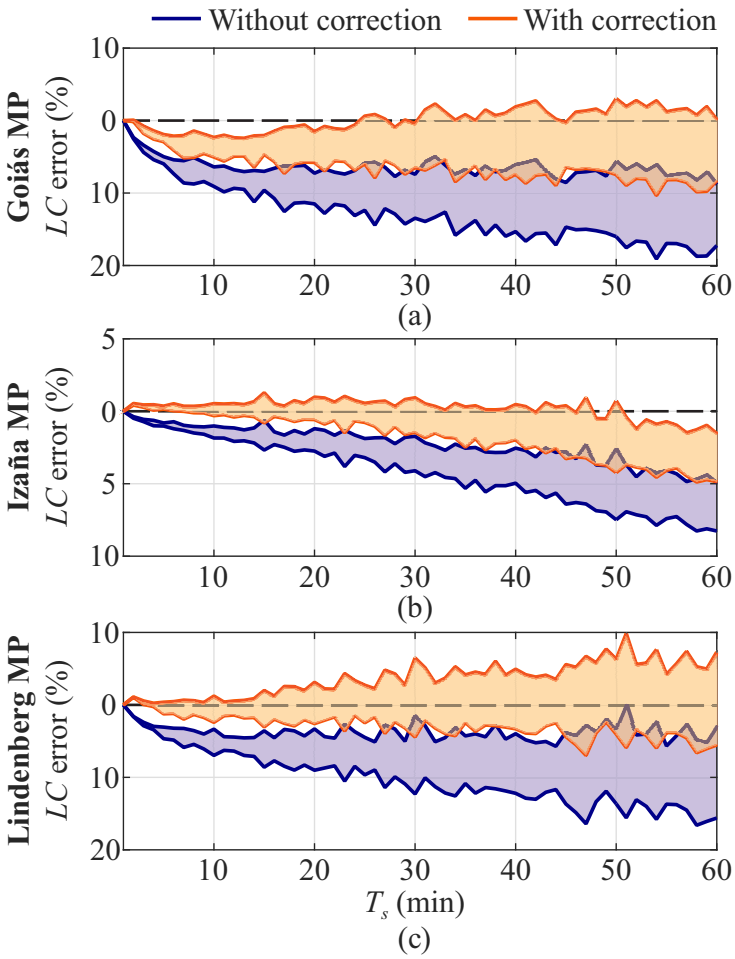

Figure 19 – Lifetime consumption errors referring to the mission profiles of: (a) Goiás, Brazil; (b) Izaña mountain, Spain and (c) Lindenberg, Germany.

for the Goiás MP and, even so, it corresponds to a reduction of approximately 45%. For T_s = 30 min, the smallest error reduction occurs for the Lindenberg MP and corresponds to a considerable decreasing of 47.27%. For T_s = 60 min, the smallest error reduction occurs for the Izaña MP and, even so, correspond to a reduction of 29.06%.

Table 5 – Lifetime consumption errors of the Goiás, Izaña and Lindenberg mission profiles in relation to the *LC* reference of each MP.

MP	T_s (min)	Error without correction (%)	Error with correction (%)	*LC* error reduction (%)
Goiás	10	9.09	5.03	44.66
	30	13.47	6.48	51.89
	60	17.25	8.28	51.94
Izaña	10	1.85	0.53	71.35
	30	4.10	1.45	64.63
	60	8.26	5.86	29.06
Lindenberg	10	6.97	2.40	65.57
	30	12.29	6.48	47.27
	60	15.62	7.29	53.33

6 Conclusions

In this work, a correction strategy to reduce the errors in the *LC* estimations of a single-phase grid-connected PV inverter caused by the MP resolution decreasing was proposed. The developed methodology aimed to determine a correction equation which is able to minimize the deviations in the *LC* estimations of a specific PV inverter when MPs with different sampling time values are used in the lifetime evaluation procedure.

For the development of the proposed methodology, the effects of the MP sampling time on the *LC* results of the power semiconductor devices and electrolytic capacitors of the dc/dc and dc/ac stages of the PV inverter were presented. The effects of the start point variations for the MP decimation process were also approached. Then, a strategy to correct the *LC* values calculated considering the short-cycle thermal loading of the dc/ac stage IGBTs of the PV inverter (which were identified as the critical-to-failure devices and more sensitive to the MP resolution) was developed and described. Finally, the calibrated correction equation determined by the proposed correction methodology was validated considering three mission profiles from different regions of the world.

As attested in this study, the *LC* spread is inherent to the proposed correction strategy. However, despite this fact, the results show that the calibrated correction equation allows to considerably reduce the deviations between the *LC* results and the *LC* references of the considered mission profiles. As observed, the maximum errors found for each MP analyzed were significantly reduced with the proposed strategy. Therefore, the proposed methodology offers an alternative for obtaining more accurate *LC* results in situations where high-resolution mission profiles are not available.

The correction equation also proved to be adaptable to the characteristics of solar irradiance and ambient temperature of different regions of the world, since it was able to improve the *LC* results of three different mission profiles. This means that the proposed correction can be performed even without the prior knowledge of the *LC* reference of the MP to be corrected. In addition, the developed methodology can be replicated for different PV inverter technologies.

References

Anurag, A.; Yang, Y.; Blaabjerg, F. Thermal performance and reliability analysis of single-phase pv inverters with reactive power injection outside feed-in operating hours. *IEEE Journal of Emerging and Selected Topics in Power Electronics*, v. 3, n. 4, p. 870–880, 2015. 27

Barros, R. C. de. *Lifetime Evaluation of Multifunctional Single-Phase PV Inverter During Harmonic Current Compensation*. Dissertação (Mestrado) — Federal Center for Technological Education of Minas Gerais, 2019. 40

Bouguerra, S. et al. The impact of pv panel positioning and degradation on the pv inverter lifetime and reliability. *IEEE Journal of Emerging and Selected Topics in Power Electronics*, p. 1–1, 2020. 27

Callegari, J. et al. Lifetime evaluation of three-phase multifunctional pv inverters with reactive power compensation. *Electric Power Systems Research*, v. 175, p. 105873, 2019. ISSN 0378-7796. 27, 40

Ciobotaru, M.; Teodorescu, R.; Blaabjerg, F. A new single-phase pll structure based on second order generalized integrator. In: *2006 37th IEEE Power Electronics Specialists Conference*. [S.l.: s.n.], 2006. p. 1–6. 31

Cupertino, A. F. et al. Impact of the mission profile length on lifetime prediction of pv inverters. *Microelectronics Reliability*, v. 100-101, p. 113427, 2019. ISSN 0026-2714. 30th European Symposium on Reliability of Electron Devices, Failure Physics and Analysis. 26, 27

Dbeiss, M.; Avenas, Y.; Zara, H. Comparison of the electro-thermal constraints on sic mosfet and si igbt power modules in photovoltaic dc/ac inverters. *Microelectronics Reliability*, v. 78, p. 65–71, 2017. ISSN 0026-2714. 27

De León-Aldaco, S. E.; Calleja, H.; Aguayo Alquicira, J. Reliability and mission profiles of photovoltaic systems: A fides approach. *IEEE Transactions on Power Electronics*, v. 30, n. 5, p. 2578–2586, 2015. 27

De León-Aldaco, S. E. et al. Effect of the mission profile on the reliability of a power converter aimed at photovoltaic applications—a case study. *IEEE Transactions on Power Electronics*, v. 28, n. 6, p. 2998–3007, 2013. 26

Esram, T.; Chapman, P. L. Comparison of photovoltaic array maximum power point tracking techniques. *IEEE Transactions on Energy Conversion*, v. 22, n. 2, p. 439–449, 2007. 32

Falck, J. et al. Reliability of power electronic systems: An industry perspective. *IEEE Industrial Electronics Magazine*, v. 12, n. 2, p. 24–35, 2018. 26

Gatla, R. k. et al. Lifetime comparison of igbt modules in grid-connected multilevel pv inverters considering mission profile. In: *2019 10th International Conference on Power Electronics and ECCE Asia (ICPE 2019 - ECCE Asia)*. [S.l.: s.n.], 2019. p. 2764–2769. 27

Golnas, A. Pv system reliability: An operator's perspective. *IEEE Journal of Photovoltaics*, v. 3, n. 1, p. 416–421, 2013. 25

Guangul, F. M.; Chala, G. T. Swot analysis of wind energy as a promising conventional fuels substitute. In: *2019 4th MEC International Conference on Big Data and Smart City (ICBDSC)*. [S.l.: s.n.], 2019. p. 1–6. 25

Hao Ma; Linguo Wang. Fault diagnosis and failure prediction of aluminum electrolytic capacitors in power electronic converters. In: *31st Annual Conference of IEEE Industrial Electronics Society, 2005. IECON 2005.* [S.l.: s.n.], 2005. p. 6 pp.–. 35

IEA. *Reliability Study of Grid Connected PV Systems: Field Experience and Recommended Design Practice*. 2002. <https://iea-pvps.org/wp-content/uploads/2020/01/rep7_08.pdf>. 26

IEA. *Renewables 2019*. 2019. <https://www.iea.org/reports/renewables-2019>. 25

IEA. *Solar PV*. 2020. <https://www.iea.org/reports/solar-pv>. 25

Lenz, J. M.; Pinheiro, J. R.; Sartori, H. C. Dc-link electrolyte capacitor lifetime analysis for a pv boost converter. In: *2017 IEEE 8th International Symposium on Power Electronics for Distributed Generation Systems (PEDG)*. [S.l.: s.n.], 2017. p. 1–6. 27, 36

Liu, H. et al. Lifetime estimation of mmc for offshore wind power hvdc application. In: *2014 International Power Electronics and Application Conference and Exposition*. [S.l.: s.n.], 2014. p. 35–40. 27

Ma, K.; Blaabjerg, F. Reliability-cost models for the power switching devices of wind power converters. In: *2012 3rd IEEE International Symposium on Power Electronics for Distributed Generation Systems (PEDG)*. [S.l.: s.n.], 2012. p. 820–827. 34, 35

Ma, K. et al. Thermal loading and lifetime estimation for power device considering mission profiles in wind power converter. *IEEE Transactions on Power Electronics*, v. 30, n. 2, p. 590–602, 2015. 34

Oh, H. et al. Physics-of-failure, condition monitoring, and prognostics of insulated gate bipolar transistor modules: A review. *IEEE Transactions on Power Electronics*, v. 30, n. 5, p. 2413–2426, 2015. 33

OLUKAN, T. A.; EMZIANE, M. A comparative analysis of pv module temperature models. *Energy Procedia*, v. 62, p. 694 – 703, 2014. ISSN 1876-6102. 6th International Conference on Sustainability in Energy and Buildings, SEB-14. 34

Pahwa, M. S.; Rahman, A. Design and estimation of reliability of an off grid solar photovoltaic (pv) power system in south east queensland. In: *2017 IEEE International Conference on Industrial Engineering and Engineering Management (IEEM)*. [S.l.: s.n.], 2017. p. 944–948. 25

Reigosa, P. D. et al. Prediction of bond wire fatigue of igbts in a pv inverter under a long-term operation. *IEEE Transactions on Power Electronics*, v. 31, n. 10, p. 7171–7182, 2016. 27, 40

REN 21. *Renewables 2020: Global Status Report*. 2020. <https://www.ren21.net/wp-content/uploads/2019/05/gsr_2020_full_report_en.pdf>. 25

Saitou, M.; Shimizu, T. Generalized theory of instantaneous active and reactive powers in single-phase circuits based on hilbert transform. In: *2002 IEEE 33rd Annual IEEE Power Electronics Specialists Conference. Proceedings (Cat. No.02CH37289)*. [S.l.: s.n.], 2002. v. 3, p. 1419–1424 vol.3. 33

Sangwongwanich, A.; Wang, H.; Blaabjerg, F. Reduced-order thermal modeling for photovoltaic inverters considering mission profile dynamics. *IEEE Open Journal of Power Electronics*, v. 1, p. 407–419, 2020. 26

Sangwongwanich, A. et al. On the impacts of pv array sizing on the inverter reliability and lifetime. *IEEE Transactions on Industry Applications*, v. 54, n. 4, p. 3656–3667, 2018. 27, 33, 34, 35, 36

Sangwongwanich, A. et al. Mission profile-oriented control for reliability and lifetime of photovoltaic inverters. *IEEE Transactions on Industry Applications*, v. 56, n. 1, p. 601–610, 2020. 26

Sangwongwanich, A. et al. Mission profile resolution impacts on the thermal stress and reliability of power devices in pv inverters. *Microelectronics Reliability*, v. 88-90, p. 1003 – 1007, 2018. ISSN 0026-2714. 29th European Symposium on Reliability of Electron Devices, Failure Physics and Analysis (ESREF 2018). 26, 28

Scheuermann, U.; Schmidt, R.; Newman, P. Power cycling testing with different load pulse durations. In: *7th IET International Conference on Power Electronics, Machines and Drives (PEMD 2014)*. [S.l.: s.n.], 2014. p. 1–6. 35

Sera, D. et al. On the perturb-and-observe and incremental conductance mppt methods for pv systems. *IEEE Journal of Photovoltaics*, v. 3, n. 3, p. 1070–1078, 2013. 32

Silva, R. et al. Pursuing computationally efficient wear-out prediction of pv inverters: The role of the mission profile resolution. *Microelectronics Reliability*, v. 110, p. 113679, 2020. ISSN 0026-2714. 26, 37, 38, 41

Sintamarean, N.-C. et al. A design tool to study the impact of mission-profile on the reliability of sic-based pv-inverter devices. *Microelectronics Reliability*, v. 54, 08 2014. 26, 27

Vernica, I.; Wang, H.; Blaabjerg, F. Impact of long-term mission profile sampling rate on the reliability evaluation of power electronics in photovoltaic applications. In: *2018 IEEE Energy Conversion Congress and Exposition (ECCE)*. [S.l.: s.n.], 2018. p. 4078–4085. 26, 28

Wang, D.; Wang, H.; Zhang, X. Mission profile-oriented configuration of pv panels for lifetime and cost-efficiency of pv inverters. *Microelectronics Reliability*, p. 113944, 2020. ISSN 0026-2714. 26

Wang, H.; Blaabjerg, F. Reliability of capacitors for dc-link applications in power electronic converters—an overview. *IEEE Transactions on Industry Applications*, v. 50, n. 5, p. 3569–3578, 2014. 35, 36

Wang, H. et al. Lifetime estimation of dc-link capacitors in adjustable speed drives under grid voltage unbalances. *IEEE Transactions on Power Electronics*, v. 34, n. 5, p. 4064–4078, 2019. 36

Xavier, L. S. *Harmonic current compensation applied in single-phase photovoltaic systems.* Dissertação (Mestrado) — Universidade Federal de Minas Gerais, 2018. 32

Yang, S. et al. An industry-based survey of reliability in power electronic converters. *IEEE Transactions on Industry Applications*, v. 47, n. 3, p. 1441–1451, 2011. 26, 33

Yang, Y.; Blaabjerg, F.; Zou, Z. Benchmarking of grid fault modes in single-phase grid-connected photovoltaic systems. *IEEE Transactions on Industry Applications*, v. 49, n. 5, p. 2167–2176, 2013. 33

Yang, Y.; Sangwongwanich, A.; Blaabjerg, F. Design for reliability of power electronics for grid-connected photovoltaic systems. *CPSS Transactions on Power Electronics and Applications*, v. 1, n. 1, p. 92–103, 2016. 25, 27

Yang, Y.; Wang, H.; Blaabjerg, F. Improved reliability of single-phase pv inverters by limiting the maximum feed-in power. In: *2014 IEEE Energy Conversion Congress and Exposition (ECCE)*. [S.l.: s.n.], 2014. p. 128–135. 27

Yazdani, A.; Iravani, R. Grid-imposed frequency vsc system: Control in -frame. In: _____. *Voltage-Sourced Converters in Power Systems: Modeling, Control, and Applications*. [S.l.: s.n.], 2010. p. 160–203. 32

Yepes, A. G. et al. Analysis and design of resonant current controllers for voltage-source converters by means of nyquist diagrams and sensitivity function. *IEEE Transactions on Industrial Electronics*, v. 58, n. 11, p. 5231–5250, 2011. 33

Zare, M. et al. Reliability assessment of single-phase grid-connected pv microinverters considering mission profile and uncertainties. In: *2017 8th Power Electronics, Drive Systems Technologies Conference (PEDSTC)*. [S.l.: s.n.], 2017. p. 377–382. 27

Zhang, G. et al. Mission profile resolution effects on lifetime estimation of doubly-fed induction generator power converter. In: *2017 IEEE Southern Power Electronics Conference (SPEC)*. [S.l.: s.n.], 2017. p. 1–6. 26, 28

Zhang, Y. et al. The impact of mission profile models on the predicted lifetime of igbt modules in the modular multilevel converter. In: *IECON 2017 - 43rd Annual Conference of the IEEE Industrial Electronics Society*. [S.l.: s.n.], 2017. p. 7980–7985. 26, 28

Zhou, D.; Blaabjerg, F. Converter-level reliability of wind turbine with low sample rate mission profile. *IEEE Transactions on Industry Applications*, v. 56, n. 3, p. 2938–2944, 2020. 27